SCIENTIFIC REPORTS
nature research

OPEN

Low temperature-calcined TiO_2 for visible light assisted decontamination of 4-nitrophenol and hexavalent chromium from wastewater

Mohamed Eid M. Ali[1*], Eman A. Assirey[2*], Shimaa M. Abdel-Moniem[1] & Hanan S. Ibrahim[1]

In the present study, alkaline hydrothermally treated titania nanoparticles (TiO_2-HT) are prepared and followed by calcination at different low temperatures to improve TiO_2 activity under visible light. The prepared photocatalysts (PCs) are characterized by different tools. TiO_2-HT is scrutinized for decontamination of para-nitrophenol (PNP) and hexavalent chromium ions (Cr^{6+} ions) under simulated sunlight. TiO_2-HT-300 and TiO_2-HT-400 PCs have nanosized particle with large surface area of 148 and 116.26 m^2/g, respectively. Additionally, XRD and FTIR proved formation of nanocrystalline anatase TiO_2. The different calcined TiO_2-HT materials show lower adsorption capacity for PNP and Cr^{6+} ions. TiO_2-HT-300 and HT-TiO_2-400 PCs have higher reduction rate of PNP than that of uncalcined temperature titania (HT-TiO_2-U) powder. Complete conversion of PNP is achieved at natural pH after 180 min over TiO_2-HT-300. As well, TiO_2-HT-300 exhibits a superior photocatalytic removal of Cr^{6+} ions. The enhanced photocatalytic efficacy is ascribed to the synergism between higher surface area and particle size (quantum effect) of TiO_2-HT-300. As results, HO· radicals are the main key active species for the photocatalytic degradation of PNP over TiO_2- HT-300 PC but contribution of O_2^- and h^+ holes is minor. The used method for preparation of TiO_2-HT-300 reduces the cost preparation as well as environmental impact reduction. Finally, low temperature-calcined TiO_2 is promising visible light active and an efficient photocatalyst with lower environmental impact for detoxification of PNP and Cr^{6+} ions from water.

As Global warming has represented a severe issue, where the protection of water sources from pollution as well as recycling of industrial effluent is essential responsibility for reducing global warming potentials. Para-nitrophenol (PNP) is extensively applied in the various manufactures; pharmaceuticals, insecticides, fungicides, drugs, and dyes. It was identified in different water streams that received industrial effluents and agricultural run-offs[1–4]. PNP and its derivatives are directly released to the environment with level that formulates risks, due to its non-biodegradability and high toxicity[5]. Upon its toxicity, persistence, and bioaccumulation to humans and animals, PNP is categorized as an emerging contaminant[6]. Human exposure to PNP induces oxygen deficiency and causes various health impacts[7–9]. PNP is considered hazardous organic pollutant. There is a serious need for its degradation from the industrialized and agricultural effluents. The removals of NPs were investigated different remediation techniques[10–18]. Herein, visible light-driven heterogeneous photocatalytic is considered and will be employed for degrading PNP; because photocatalysis technology is an eco-friendly, green and sludge free remediation technique. The lowering of calcination temperature reduces the environmental impact of preparation process via decreasing the electricity consumption. We supposed that the lower size particles (quantum dot effect), high surface area, surface morphology and lowering band gap have important effects on the photocatalytic performance. Previously, the efficiency of TiO_2 under visible light was chiefly enhanced by ions coupling, existence of different phases, or configuration[19–22]. These trends are costly and complicated. Therefore, the study aimed to

[1]Water Pollution Research Department, National Research Centre, 33 El-Behouth St., Dokki, Cairo, Egypt, P.O. 12622. [2]Chemistry Department, Taibah University, Medinah, Kingdom of Saudi Arabia, P.O. 4744. *email: alienv81@yahoo.com; eman_assirey@hotmail.com

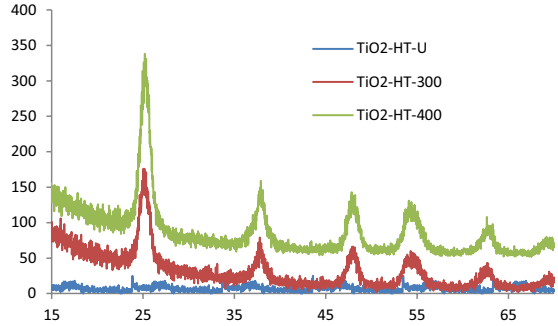

Figure 1. XRD pattern of different prepared photocatalysts.

improve TiO_2 via modification of surface area and particle size using facile and simple hydrothermal treatment under alkaline conditions without introduction of metal or non-metal to titania. In this work, TiO_2 is synthesized using hydrothermal procedure in alkaline media to control surface area and particle size and applied for decontamination of PNP and hexavalent chromium from wastewaters.

Results and Discussion

Characterization of photocatalyst. Powder XRD used to investigate the existence of different crystallographic phase of the prepared materials. The XRD patterns of TiO_2-HT that prepared by hydrothermal refluxing with alkaline solution followed with calcination at different temperatures (105, 300, 400 °C) are shown in Fig. 1. Hydrothermally treated TiO_2 sample without post-heating (TiO_2-HT-U) showed no diffraction peaks indicating amorphous structure of TiO_2. The diffraction peaks for TiO_2-HT-300 and TiO_2-HT-400 are well concurring with those of the standard data (**JCPDS card no. 21-1272**) and has a superior crystalline structure with hexagonal anatase phase and no additional peaks related to rutile phase of TiO_2 are noticed. Moreover, the calculated d-spacing of 3.53 Å for dominant diffraction line is consistency with the spacing of (101) plane hexagonal anatase phase. The average crystallite size for TiO_2-HT-300 and TiO_2-HT-400 was determined by Scherrer equation[23], it was found to be 8.34 and 10.34 nm, respectively. Furthermore, the reflection width is considerably broadened indicating a small nanocrystalline size which is essential for enhancing the photocatalytic activity of material for degrading the aqueous pollutants.

FTIR spectra analysis for HT-TiO_2 PC. FTIR spectra of prepared TiO_2-HT-300 and TiO_2-HT-400 materials are analyzed to identify the functional active groups on the surface and showed in Fig. S2. Due to OH stretching vibration, a wide IR band is perceived between 3200 to 3600 cm^{-1} [24,25]. The wide absorption region below 1000 cm^{-1} is due to the vibration of the Ti-O and Ti-O-Ti bond. The peaks around 1260 and 1430 cm^{-1} in spectra are ascribed to anatase O-Ti-O bonding and Ti-OH and adsorbed water in TiO_2. These findings confirm the presence of anatase titania.

N_2-adsorption/desorption analysis for HT-TiO_2 PC. Furthermore, N_2 adsorption/desorption analysis of different prepared HT-TiO_2 is investigated for finding out porosity and surface area and illustrated in Fig. 2. As shown Fig. 2(a,b), adsorption/desorption isotherms for TiO_2-HT-300 and TiO_2-HT-400 are similar to IUPAC isotherm III with H3 hysteresis loop in the relative pressure range from 0.2–0.92 indicating mesoporous structure of the prepared material. Figure (2c,d) display the pore size distribution ranges from 1.9 to 13 nm for TiO_2-HT-300 and TiO_2-HT-400 samples from 1.95 to 34 nm with corresponding average pore size and pore volume are 3.5 and 6.5 nm, and 0.22 and 0.213 cm^3/g, respectively. The obtained mesoporosity for TiO_2-HT-300 and TiO_2-HT-400 is ought to hydrothermal treatment. The pores TiO_2-HT-300 and TiO_2-HT-400 samples ought to condensation of adsorbed water as shown Fig. 2c,d. The specific surface areas are 149 and 116 m^2/g for TiO_2-HT-300 and TiO_2-HT-400, respectively. The higher surface area is due to existence of more pores. The lowering of surface area for TiO_2-HT-400 is attributed higher temperature of calcination. The superior specific surface area and porous structure of TiO_2-HT-300 proffer more interfacial sites available for the photocatalytic reaction and thus improve the effectiveness. The photocatalytic activity of prepared materials will be discuss later.

Scanning electron microscopy (SEM) for TiO_2-HT PC. SEM is an awfully practical mean for investigation of the surface morphology of TiO_2 nanoparticle. Figure S3 showed the morphological surfaces of different calcined TiO_2-HT. Fig. (S3a-b) reveals no existence of definite shape and distribution for TiO_2-HT-U. But Figures (S3c–e,f-h) depicted homogeneous and uniform distributed particles with nanosized spherical shaped material for TiO_2-HT-300 and TiO_2-HT-400, respectively which is consistent with XRD result findings.

Transmission Electron Microscope (TEM) for TiO_2-HT-PC. The typical TEM images of TiO_2-HT with different calcination temperature are depicted in Fig. 3(a–f). Figure 3(a,b) reveals an indefinite crystalline structure for TiO_2-HT-U, which is consistent with XRD results. Figure 3(c,d,e,f) showed aggregated spherical shape with particle size ranged between 8.3 to 10.4 nm for TiO_2-HT-300 and 13.5 to 18.4 nm for TiO_2-HT-400. As well these finding are in consistence with XRD data. High resolution transmission microscopy (HR-TEM) is carried out on higher photoactive materials TiO_2-HT-300, Fig. 3(g,h) revealed 2D structure TiO_2-HT-300 with existence definite interplanar spacing of 0.35 nm which ascribed to 101 plane of anatase TiO_2. These finding somehow

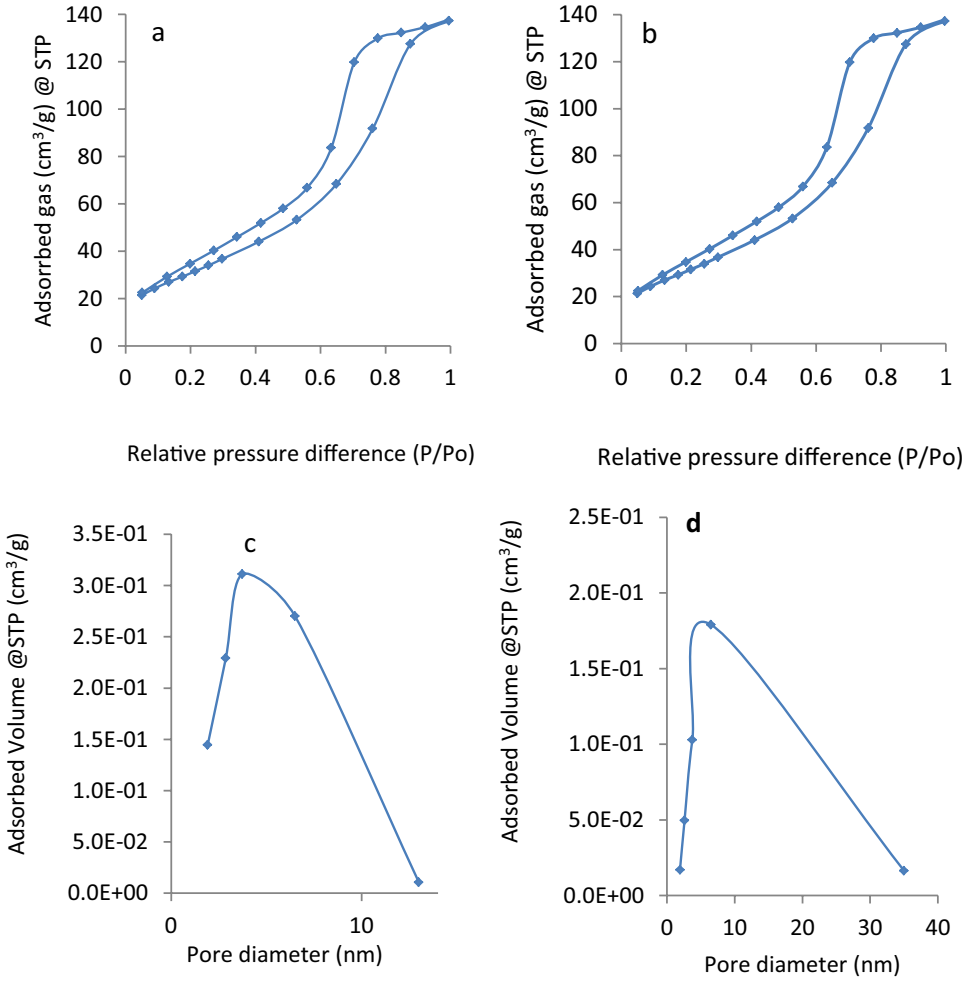

Figure 2. Isotherm of TiO_2-HT-300 (**a**) and TiO_2-HT-400 (**b**), pore distribution of TiO_2-HT-300 (**c**) and TiO_2-HT-400 (**d**).

demonstrate the consistence with XRD results. Figure 3i showed SEAD and reveals confirming polycrystalline characteristic of TiO_2PC.

Particle size distribution for HT-TiO_2 PC. Figure 4(a,b) showed the uniform distribution of particle for size TiO_2-HT-300 and TiO_2- HT-400. It reveals with particle size between 4 to 20 nm for TiO_2-HT-300 with average of 8 nm and as well TiO_2-HT-400 PC shows particles size of 7–30 nm with average size of 13 nm. These findings of particle size are in agreement with size estimation from TEM the XRD analysis for crystalline size.

Optical properties for HT-TiO_2 PC. UV–Vis absorption was utilized to estimate the optical characteristics of prepared TiO_2- HT-300 photocatalysts comparing with commercial TiO_2 and (Fig. 4c,d). The absorption (A) is shifted to lower energy light (i.e. longer wavelength) for HT-TiO_2-300 sample than that of commercial titania (TiO_2-C). Hence, TiO_2-HT-300 samples have become more active in near visible light region. Kubelka–Munk function was employed to estimate the bandgap energy (Eg) from optical spectra of PC[26]. The relation between hυ and $(h\upsilon\, F(R))^{1/2}$ is depicted for HT-TiO_2-300 and TiO_2-C in Fig. 4(c,d). The band gap energies of TiO_2-C and TiO_2-HT-300 samples were 3.22 and 3.09 eV, respectively. These results reveal increasing visible light harvesting by TiO_2-HT-300. The more absorption wavelength range is, the higher the formation rate of electron–hole pairs on the photocatalyst surface increased. Moreover, greatly sequentially more free radicals as well as hydroxyl radicals/holes are produced in solution and improved the degradation activity of PC[27].

Photocatalytic activity of prepared photocatalysts. The photocatalytic removal of PNP (20 mg. L^{-1}) over different calcined TiO_2-HT PC with dose of 0.5 g/L is investigated. Time profile of removal of PNP from aqueous solution is plotted over different calcined TiO_2-HT under irradiation with visible light (solar simulator) and Fig. 5a. Since, PNP decomposition under visible light irradiation without catalysts was negligible. Meanwhile, the dark adsorption achieved only 3.0–6.3% removal rate over different TiO_2-HT. It remarkably noticed that TiO_2-HT-300 and TiO_2-HT-400 PCs reduced PNP concentration with rate faster than that found for HT-TiO_2-U powder. Where, only 38% of PNP is reduced after 180 min, it could be owed to uncrystallinity of TiO_2-HT-U. After 120 min, the superior photocatalytic removal (95%) of PNP is achieved for HT-TiO_2-300 which higher than

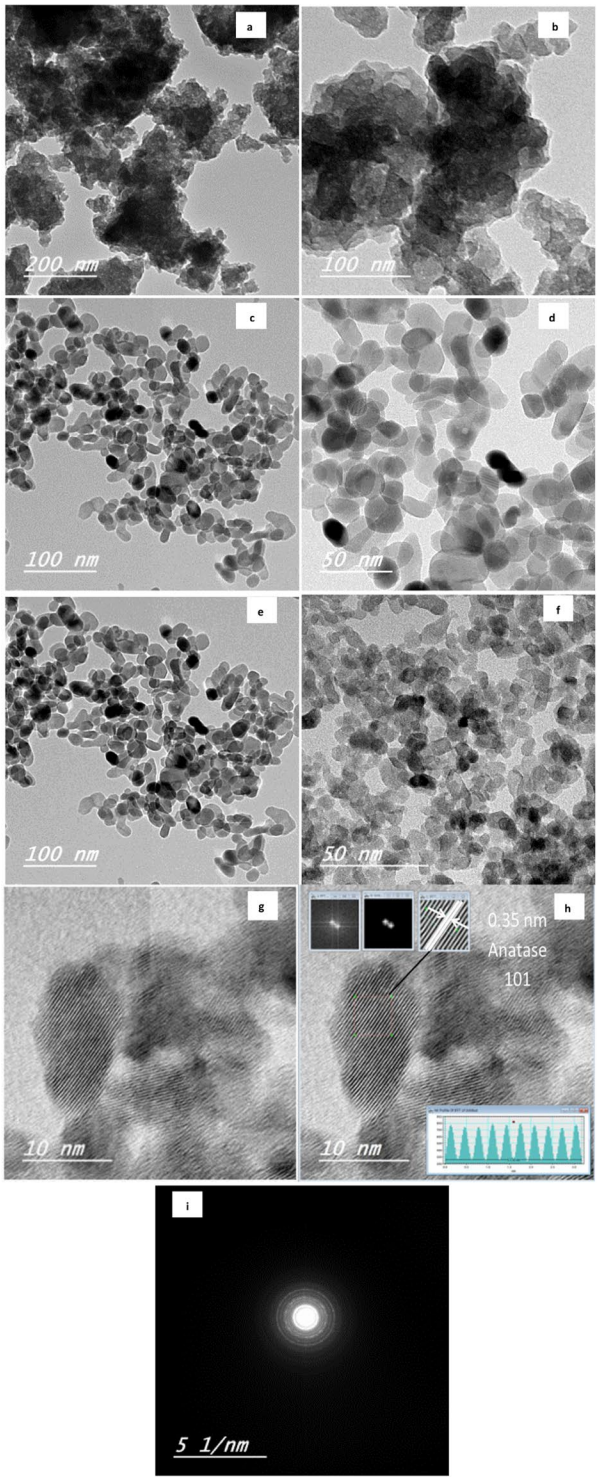

Figure 3. TEM mage of TiO_2-HT-U (**a,b**), TiO_2-HT-300 (**c,d,g,h,i**) and TiO_2-HT-400 (**e**,**f**).

that of HT-TiO_2-400 under visible light (ca. 60%). However, complete reduction of PNP is achieved after 180 min using TiO_2- HT-300, but only 85% of PNP is removed over TiO_2-HT-400 under visible light. The results pointed out the importance of calcination treatment of hydrothermally treated TiO_2. Overall, TiO_2-HT-300 exhibits a superior activity for degradation of PNP. Consequently, the improved photocatalytic efficacy is endorsed to the synergism of higher surface area and small particle size of TiO_2-HT-300 with photodegradation activity of photocatalyst[28]. The higher surface area of TiO_2-HT-300 results in more adsorption and photocatalytic activity compared to TiO_2-HT-400 and TiO_2-HT-U. It was revealed that the surface area is supposed as the foremost parameter affecting the photocatalytic activity, where the greater surface area introduces, the more active sites for light harvesting as well as photocatalytic process are, which improves the photocatalytic activity (Abdel

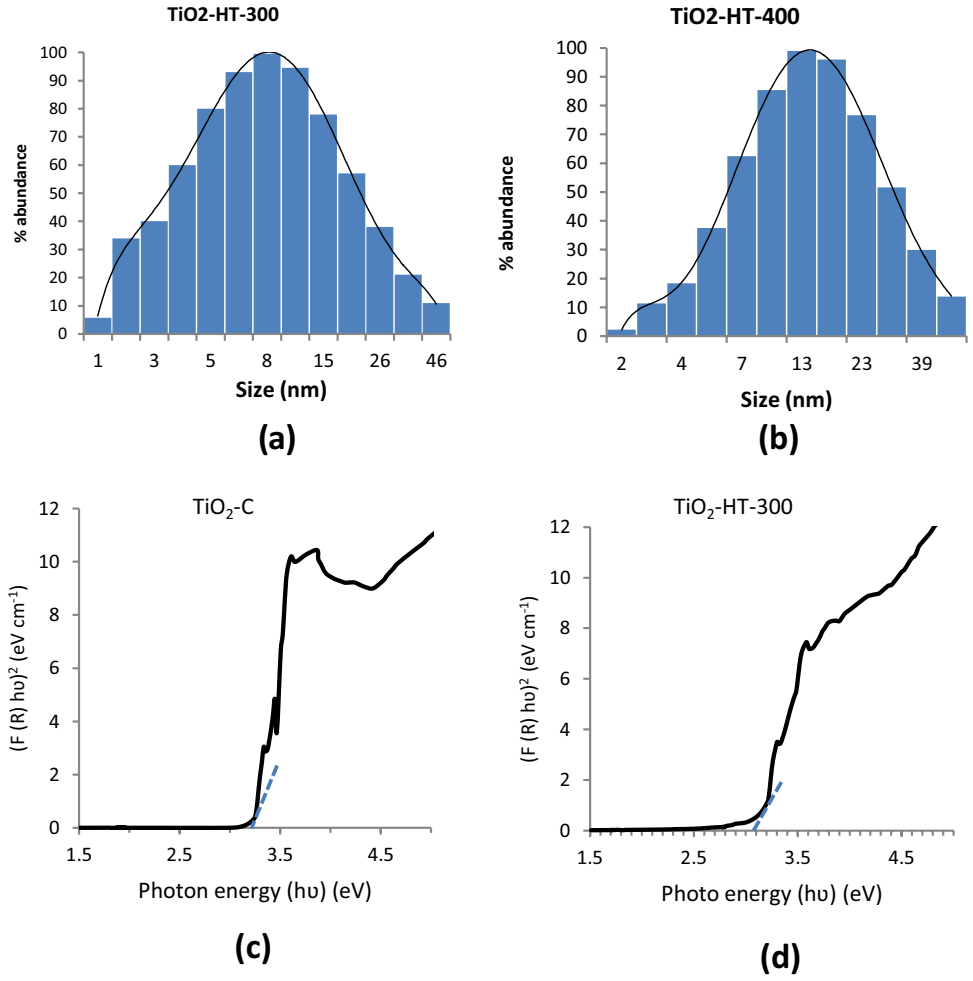

Figure 4. Particle size distribution for TiO_2-HT-300 (**a**), and TiO_2-HT-400 (**b**), Optical properties of prepared photocatalysts for TiO_2-C (**c**), and TiO_2-HT- 300 (**d**).

Moniem *et al*., 2015; Badawy *et al*., 2015). Moreover, TiO_2-HT-300 has quantum dot nanoparticle (8.5–10.5 nm) that possibly facilitates the charge separation and prevents recombination of electron–hole pairs[24,25]. As well it is hypothesized that TiO_2-HT-300 possesses more photocatalytic activity under visible-light, which in consistence with optical properties (See Fig. 4d). Where, the degradation efficiency is enhanced due to decreasing the band gap values of HT-TiO_2-300 which valorizes the more absorption of visible light leads to more production of free radicals and reactive oxidizing species.

In the current study, TiO_2-HT-300 PC activity is efficient for PNP removal under solar simulator, that is comparable or higher than that of the previous results. Many PCs were applied for removal of PNP under visible light; TiO_2, PW12/TiO_2, 20% g-C_3N_4/TiO_2 and ternary photocatalyst composite of PW12/TiO_2/g-C_3N_4 with dose of 1 g/L and PNP concentration of 20 mg.L^{-1}, the conversion of PNP reaches 10%, 20%, 70% and 98.6% under visible-light irradiation, respectively[29]. As well, Ag-AgBr-RGO catalyst is efficient for complete degradation of 5 mg/L of PNP after 180 min of visible light irradiation[30]. Also, over 2 g/L of Bi_2O_3 PC, maximum of 100% degradation of PNP within 90 min was achieved meanwhile only 35%, 34% and 22% of PNP was degraded under visible light using TiO_2, ZnO, and ZrO_2, respectively within 90 min[31].

For attainment a good assessment between photocatalytic performances of different hydrothermally treated TiO_2, the decomposition rate constants (*kapp*) over the samples are computed using pseudo-first-order kinetic model and the data are displayed in Fig. S4. The results revealed that *kapp* for photocatalytic degradation of PNP rate constant are 1.9×10^{-3}, 7.6×10^{-3}, and 23.2×10^{-3} min^{-1} for TiO_2-HT-U, TiO_2-HT-300 and TiO_2-HT-400 PC, respectively. Obviously, the degradation rate constant of PNP over the TiO_2-HT-300 and TiO_2-HT-400 PC is 12.2 and 4 folds higher than that for TiO_2-HT-U and TiO_2-HT-400, respectively. It was obviously revealed that TiO_2-HT-300 has noticeably better photocatalytic efficiency. This improved is confirmed by TEM, optical properties, particle distribution, and BET surface analyses.

Generally, the photoinduced activated species such as entrapped holes (h^+), hydroxyl radicals ($^{\bullet}OH$) and superoxide radical anions (O_2^-) have roles in the photocatalytic process[32]. Moreover, the determining the contributing reactive species in the photocatalytic process is important to investigate the mechanism of the photocatalytic process of PNP degradation. The main active species generated during the photocatalytic destruction process of PNP are scrutinized by entrapping trial. As shown in Fig. 5b, it is found that the removal rates of PNP

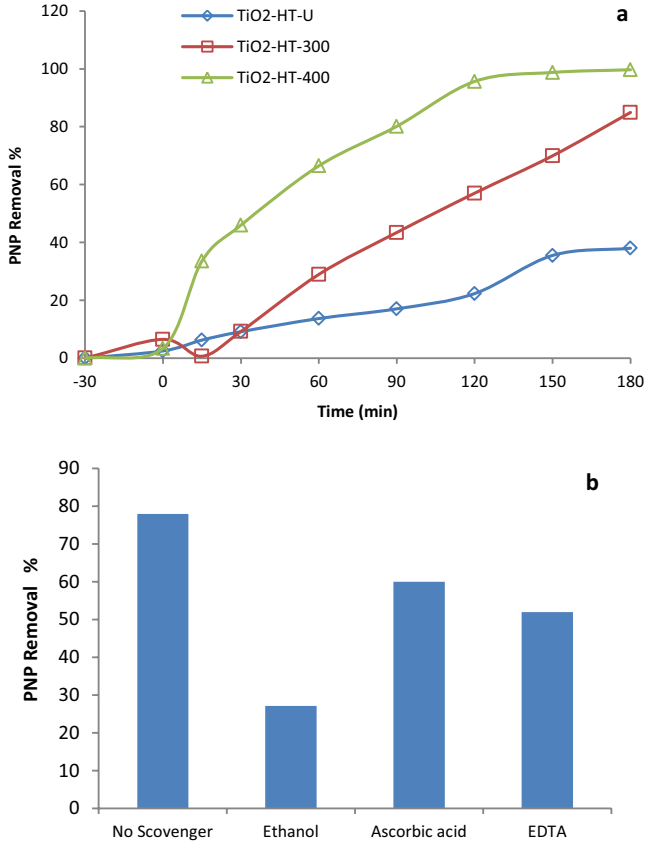

Figure 5. (**a**) Photocatalytic activity of different calcined TiO_2-HT for photocatalytic removal of 4 NP (Photocatalyst dose 0.5 g/L, PNP concentration 20 mg. L^{-1}), (**b**) The photocatalyzed reduction of PNP with different scavenger under visible light irradiation after 90 min over TiO_2-HT-300.

degradation are reduced to 27, 60 and 52% upon introducing ethanol (•OH radical scavenger), ascorbic acid ($O_2^{-\bullet}$ radical scavenger) and EDTA (hole scavenger), respectively. Evidently, the introducing ethanol as •OH radicals scavenger, gives a sharp reduction photocatalyzed removal effectiveness to 27%, entail that the free •OH radicals has the major effect on PNP degradation. Meanwhile, in presence of ascorbic acid and EDTA, the photodegrading rate of PNP was slightly decreased, which reveals that the holes and $O_2^{-\bullet}$ radical are subsidiary contributor in the photocatalytic removal of PNP. Therefore, •OH radicals are main key active species for the photocatalytic degradation of PNP over TiO_2-HT-300 PC which afford strong indication for the higher photocatalytic ability of TiO_2-HT-300.

The detoxification of 20 mg. L^{-1} of Cr^{6+} from aqueous solution was investigated using TiO_2-HT-U, TiO_2-HT-300 and TiO_2-HT-400; PCs and 60 mg. L^{-1} of formic acid for 180 min under sunlight simulator (UVACUBE 400) and the removal results of Cr^{6+} ions via adsorption and photocatalysis over different TiO_2-HT. Dark adsorption trials are carried out for 30 min to get adequate adsorption of Cr^{6+} ions on the surface of PCs. It was found that only 13% and 9% of Cr^{6+} ions are removed over TiO_2-HT-300 and TiO_2-HT-400, respectively. No adsorption activity is noticed for TiO_2-HT-U. Control experiment was done without introducing PC in presence of formic acid and no Cr^{6+} ions is remarkable reduced, which revealed that the spontaneous photoreduction of Cr^{6+} ions under visible light is negligible. Figure 6a displayed the photocatalytic reduction curves of Cr^{6+} ions over TiO_2-HT-U, TiO_2-HT-300 and TiO_2-HT-400 PCs. The results showed that Cr^{6+} ions photoreduced by 17%, 89% and 59% after 60 min over TiO_2-HT-U, TiO_2-HT-300 and TiO_2-HT-400 PCs, respectively. Meanwhile, the corresponding noticed photoreduction percentages are 99%, 73% and 23% after 90 min. The photocatalytic reduction efficiency of Cr(VI) ions increases in the order of TiO_2-HT-300 > TiO_2-HT-400 > TiO_2-HT-U after 90 min of simulated sunlight light irradiation. As above mentioned, TiO_2-HT-300 has the higher proficient activity for photoreduction of Cr^{6+} ions due to separation of photo-generated electron– hole pairs via quantum dots of PC effect, higher surface area and lower bandgap energy (Eg = 3.09 eV). Photoreduction kinetics of Cr^{6+} ions are investigated over different calcined TiO_2-HT and the time profile of Ln (C/C_0) illustrated in Fig. 6b. The data showed that *kapps* for photocatalytic degradation of Cr^{6+} ions are 2.9×10^{-3}, 36.3×10^{-3}, and 14.8×10^{-3} min^{-1} for TiO_2-HT-U, TiO_2-HT-300 and TiO_2-HT-400, respectively. Obviously, the removal rate constant of Cr^{6+} ions over the TiO_2-HT-300 and TiO_2-HT-400 PC is 12.5 and 2.5 folds higher than that for TiO_2-HT-U, TiO_2-HT-400, respectively.

Based on data (**as shown** Table S1), the photoreduction rate constants (*kapp*) and initial removal rate (r_0) of Cr^{6+} ions are higher than that of PNP. Upon visible light irradiation of TiO_2-HT, the adsorbed photon separated electrons-holes pairs (See Fig. 7). Then, electrons transferred to conduction band and shifted toward the surface

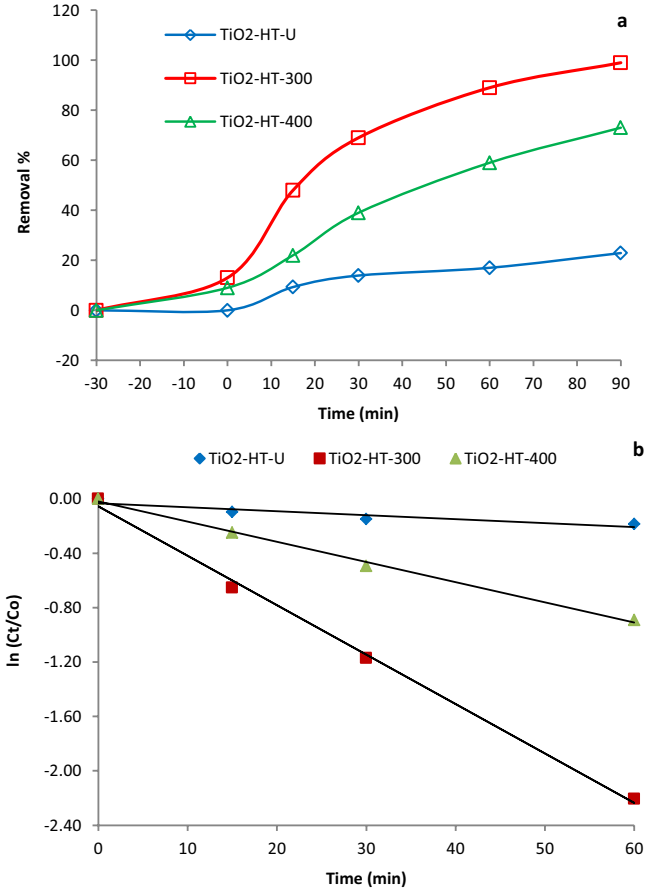

Figure 6. Photocatalytic reduction of Cr^{6+} ion over different PCs under visible light irradiation (**a**), PFO kinetic model (**b**) (Photocatalyst dose 0.5 g/L, Cr^{6+} concentration 20 mg. L^{-1}).

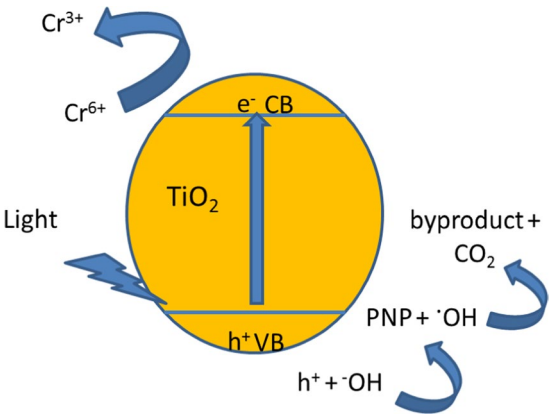

Figure 7. Mechanism of photocatalytic reduction of Cr^{6+} ion and PNP over TiO_2-HT PC under visible light irradiation.

of PC leading to reduce Cr^{6+} ions directly in case of photoreduction[29]. In case of photocatalytic oxidation, the holes are left in valence band which react with water or hydroxide ions to produce hydroxyl radicals (•OH). After that, PNP degraded by •OH attack which will consume more time rather than direct reduction of Cr^{6+} ions. Conclusively, the alkaline hydrothermal treatment for titania with proper calcination temperature possibly improves the photoactivity under sunlight illumination and decontamination of waters from various pollutant; PNP and Cr^{6+} ions. As well, the lower calcined-temperature TiO_2-HT showed good efficiency rather than the higher calcined-temperature, which results in reduces the energy consumption during the preparation process of materials. Thus, the environmental impact due to electricity use is decreased. Application of TiO_2-HT-300 is sustainable approach for detoxification of PNP and Cr^{6+} ions from waters.

Conclusion

Low temperature-calcined titania nanoparticles (TiO_2-HT) was synthesized for increasing photocatalytic efficiency of TiO_2 under visible light. The prepared photocatalysts (PC) is characterized by different techniques. HT-TiO_2 is employed for photocatalyzed decontaminating PNP and Cr^{6+} ions under solar simulator. The obtained results revealed existence of nanosized particle with large surface area. As result, formation nanocrystalline anatase TiO_2 confirmed XRD and FTIR data. Based on DRS data, hydrothermally treated TiO_2 become near-visible light photoactive for depollution. Lower fractions of PNP and Cr^{6+} ions are adsorbed over different TiO_2-HT PCs. TiO_2-HT-300 and TiO_2-HT-400 PCs have higher reduction rate of PNP and Cr^{6+} ions under solar simulator. Using solar-driven photoreaction, TiO_2-HT-300 shows complete removal for PNP and Cr^{6+} ions after 180 min and 90 min, respectively. Photoreduction rate constant of Cr^{6+} ions over TiO_2-HT-300 is 2.5 and 12.5 times higher than that of TiO_2-HT-400 and TiO_2-HT-U, respectively. The synergism of higher surface area and small particle size enhanced photocatalytic efficacy for photodegradation of PNP. As consequences, $^{\cdot}OH$ radicals are major active species for the photocatalytic degradation of PNP over TiO_2-HT-300. The applied method for TiO_2-HT-300 preparation decreases the cost preparation and environmental impact reduction due to lowering calcination temperature as well as electricity consumption. As well finally, low temperature-calcined TiO_2 with solar-driven photoreactor is new approach for detoxification of PNP and Cr^{6+} ions from water/wastewater.

Experimental

Preparation of TiO_2 -HT photocatalyst. Titanium hydroxide gel was synthesized as stated previously[23], The resulted gel was then dried to make $Ti(OH)_4$. To prepare hydrothermally treated titania (TiO_2-HT), four grams of hp-$Ti(OH)_4$ were suspended in 100 mL of 2 M NaOH aqueous solution. This suspension was stirred during 60 min at room temperature and the mixture was transferred into round flask, and then was refluxed for 24 h at 160 °C. The obtained material was washed with H_2O and filtered off. This washed material was suspended in 500 mL of aqueous solution of HCl (0.1 N) and stirred for 24 h. The treatment with HCl was repeated 3 times in order to remove the residual sodium ions. Then, the materials were washed with deionized water several times to remove chloride. These formed materials were dried in oven at 105 °C. Finally, the prepared powders were calcined at different temperatures. The prepared catalysts were denoted with TiO_2 HT–U, TiO_2- HT-300 and TiO_2-HT-400 for catalyst and treated at temperature of 105, 300 and 400 °C, respectively.

Characterization of HT-TiO_2 PC. The characterization of materials are previously described[24,26,28], powder X-ray diffraction (XRD) was performed on a PANalytical X'PertPRO X-ray diffractometer using filtered Cu Kα radiation ($\lambda = 0.154$ nm). Fourier transform infrared (FTIR) spectroscopy was conducted by using a BRUKER VERTEX 70. Transmission electron microscopy (TEM) images were taken using a JEOL JSM-1200 EX II operating at 100 kV. Scanning electron microscopy (SEM) images were taken using a JEOL JSM-7600F field emission scanning electron microscope. High-resolution transmission electron microscopy (HRTEM) images were taken with a Tecnai 20 G2S-Twin operating at 200 kV. Nitrogen adsorption–desorption isotherms were measured at 77 K with a Micromeritics ASAP 2010. The specific surface areas were calculated by the Brunauer–Emmett–Teller (BET) method. Zeta-potential analysis was performed on a Malvern Zetasizer Nano ZS. DSR spectra were obtained in air at ca. 300 K in the wavelength range 200–900 nm using a Shimadzu UV-2401 PC spectrophotometer with $BaSO_4$ as the reference material.

Photocatalytic Activity for HT-TiO_2 PC. A Pyrex batch reactor of beaker with volume of 250 mL, was used for performing the reactivity experiments. Illumination is provided by solar simulator UVACUBE 400, Honle, Germany. The photocatalytic activity of prepared photocatalyst is tested by reactions of photo-degradation of 4-nitrophenol. 100 ml of 20 ppm of pollutant (PNP, Cr^{6+} ions) was added to photoreactor. The photocatalyst of 50 mg was suspended in 100 ml of aqueous solution of pollutant and then stirred for 30 min to make the photocatalyst homogeneously dispersed into the solution of reaction. Then, the solar simulator was turned on, sample were taken at time interval. The concentration of 4-nitrophenol and Cr^{6+} ions are analyzed by a JASCO- V-730, UV–Visible recording spectrophotometer at $\lambda_{max} = 318$ and 350 nm, respectively. Before determination, the withdrawn suspensions are filtered with syringe filter (Whatman, 0.45 µm). The pathway of photocatalytic mechanism is investigated in presence of ethanol, ascorbic acid (AA), and ethylene diamine tetra acetate (EDTA) with concentration (2 mM) for each one as $^{\bullet}OH$ radical, $O_2^{-\bullet}$ radical and holes scavengers, respectively.

Received: 30 September 2019; Accepted: 28 November 2019;
Published online: 18 December 2019

References

1. Wang, Q. *et al*. Facile and rapid microwave-assisted preparation of Cu/Fe-AO-PAN fiber for PNP degradation in a photo-Fenton system under visible light irradiation. *Sep. Purif. Technol.* **209**, 270–278 (2019).
2. Sun, Y., Zhou, J., Cai, W., Zhao, R. & Yuan, J. Hierarchically porous NiAl-LDH nanoparticles as highly efficient adsorbent for p-nitrophenol from water. *Appl. Surf. Sci.* **349**, 897–903, https://doi.org/10.1016/j.apsusc.2015.05.041 (2015).
3. Zarei, A. R., Rezaeivahidian, H. & Soleymani, A. R. Investigation on removal of p-nitrophenol using a hybridized photo-thermal activated persulfate process: Central composite design modeling. *Process Saf. Environ. Prot.* **98**, 109–115 (2015).
4. Zhang, H., Fei, C., Zhang, D. & Tang, F. Degradation of 4-nitrophenol in aqueousmedium by electro-Fenton method. *J. Hazard. Mater.* **145**, 227–232 (2007).
5. Yu, S. Q., Hu, J. & Wang, J. L. Gamma radiation-induced degradation of p-nitrophenol (PNP) in the presence of hydrogen peroxide (H_2O_2) in aqueous solution. *J. Hazard Mater.* **177**, 1061–1067 (2010).
6. Atieh, M. A. Removal of phenol from water different types of carbon—a comparative analysis. *APCBEE Procedia.* **10**, 136–141, https://doi.org/10.1016/j.apcbee.2014.10.031 (2014).
7. Labana, S. *et al*. Pot and field studies on bioremediation of p-nitrophenol contaminated soil using Arthrobacter protophormiae RKJ100. *Environ. Sci. Technol.* **39**, 3330–3337, https://doi.org/10.1021/es0489801 (2005).

8. Liu, Z., Yang, C. & Qiao, C. Biodegradation of p-nitrophenol and 4-chlorophenol by *Stenotro-phomonas* sp. *FEMS Microbiol. Lett.* **277**, 150–156, https://doi.org/10.1111/j.1574-6968.2007.00940.x (2007).
9. Xue, G., Gao, M., Gu, Z., Luo, Z. & Hu, Z. The removal of p-nitrophenol from aqueous solutions by adsorption using gemini surfactants modified montmorillonites. *Chem. Eng. J.* **218**, 223–231, https://doi.org/10.1016/j.cej.2012.12.045 (2013).
10. Yang, J. *et al*. Degradation of p- Nitrophenol on biochars: role of persistent free radicals. *Environ. Sci. Technol* **50**, 694–700 (2015).
11. Gupta, V. K., Atar, N., Yola, M. L. & Uzun, L. A novel magnetic Fe@Au core shell nanoparticles anchored graphene oxide recyclable Nano catalyst for the reduction of nitro- phenol compounds. *Water Res.* **482**, 10–217 (2014).
12. Aktas, O. & Ferhan, C. Adsorption and co-metabolic bio-regeneration in activated carbon treatment of 2-nitrophenol. *J. Hazard Mater.* **177**, 956–961 (2010).
13. Koubaissy, B., Joly, G. & Magnoux, P. Adsorption and competitive adsorption on zeolites of nitrophenol compounds present in wastewater. *Ind. Eng. Chem. Res* **47**, 9558–9565 (2008).
14. Kuosa, M., Laari, A., Solonen, A., Haario, H. & Kallas, J. Multicomponent reaction kinetics for the ozonation of para-nitrophenol and its decomposition products under acidic conditions at constant pH. *Chem. Eng. Sci.* **64**, 2332–2342 (2009).
15. Kulkarni, P. Nitrophenol removal by simultaneous nitrification denitrification (SND) using T. pantotropha in sequencing batch reactors (SBR). *Bioresour. Technol.* **128**, 273–280 (2013).
16. Pradhan, A. A. & Gogate, P. R. Removal of p-nitrophenol using hydrodynamic cavitation and Fenton chemistry at pilot scale operation. *Chem. Eng. J.* **156**, 77–82 (2010).
17. Oturan, M. A., Peiroten, J., Chartrin, P. & Acher, A. J. Complete destruction of p-nitrophenol in aqueous medium by electro-Fenton method. *Environ. Sci. Technol.* **34**, 3474–3479 (2000).
18. Sahoo, N. K., Pakshirajan, K. & Ghosh, P. K. Batch biodegradation of para-nitrophenol using arthrobacter chlorophenolicus A6. *Appl. Biochem. Biotechnol.* **165**, 1587–1596 (2011).
19. Khalid, N. R., Ahmed, E., Hong, Z. & Ahmad, M. Synthesis and photocatalytic properties of visible light responsive La/TiO_2-graphene composites. *Appl. Surf. Sci.* **263**, 254–259, https://doi.org/10.1016/j.apsusc.2012.09.039 (2012).
20. Sun, X. *et al*. Ce-doped SiO_2@TiO_2 nanocomposite as an effective visible light photocatalyst. *J. Alloys Compd.* **585**, 800–804, https://doi.org/10.1016/j.jallcom.2013.10.034 (2014).
21. Yasmina, M., Mourad, K., Mohammed, S. H. & Khaoula, C. Treatment heterogeneous photocatalysis; Factors influencing the photocatalytic degradation by TiO_2. *Energy Procedia* **50**, 559–566, https://doi.org/10.1016/j.egypro.2014.06.068 (2014).
22. Pan, L., Zhang, X., Wang, L. & Zou, J. J. Controlling surface and interface of TiO2 toward highly efficientphotocatalysis. *Mater. Lett.* **160**, 576–580 (2015).
23. Badawy, M. I., Ali, M. E. M., Ghaly, M. Y. & El-Missiry, M. A. Mesoporous simonkolleite–TiO2 nanostructured composite for simultaneous photocatalytic hydrogen production and dye decontamination. *Process Safety and Environmental Protection* **94**, 11–17 (2015).
24. Ali, M. E. M., Abdelsalam, H., Ammar, N. S. & Ibrahim, H. S. Response surface methodology for optimization of the adsorption capability of ball-milled pomegranate peel for different pollutants. *J. Mol. Liq.* **250**, 433–445 (2018).
25. Assirey, E. A. R. *et al*. Novel Composite for Lead Ions Removal from Wastewater. *Journal of Computational and Theoretical Nanoscience* **14**, 5735–5742 (2017).
26. Abdel Moniem, S. M. *et al*. Detoxification of hexavalent chromium in wastewater containing organic substances using simonkolleite-TiO_2 photocatalyst. *Proc. Safe. Environ. Protect.* **95**, 247–254 (2015).
27. Ali, M. E. M., Alhathal Alanezi, A., Azeez, F. A. & Ghaly, M. Y. Photoassisted mineralization of remazole red F3B over NiO/TiO_2 and CdO/TiO_2 nanoparticles under simulated sunlight. *Sep. Sci. Technol., (Philadelphia)* **53**, 170–180 (2018).
28. Badawy, M. I., Ghaly, M. Y. & Ali, M. E. M. Photocatalytic Hydrogen Production over Nano-structured Mesoporous Titania from Olive Mill Wastewater. *Desalination* **267**(2-3), 250–255 (2011).
29. L Li, *et al*, Novel $H_3PW_{12}O_{40}$/TiO_2-g-C_3N_4 type-II heterojunction photocatalyst with enhanced visible-light photocatalytic properties, J. of Solid State Chem. 274, 152–161 (2019).
30. Yang, Y., Zhang, W., Liu, R., Cui, J. & Deng, C. Preparation and photocatalytic properties of visible light driven Ag-AgBr- RGO composite. *Sep. Purif. Technol.* **190**, 278–287 (2018).
31. Muersha W., Soylu G.S.P, Effects of metal oxide semiconductors on the photocatalytic degradation of 4-nitrophenol J. of Molecular Structure, 1174, 96–102 (2018).
32. Zhang, J. & Nosaka, Y. Mechanism of the OH Radical Generation in Photocatalysis with TiO_2 of Different Crystalline Types. *J. Phys. Chem. C* **118**(20), 10824–10832 (2014).

Author contributions

Ali and Abdel-Monein carried out the experimental work; preparation of PC and photocatalytic activity assessment. Ali wrote the characterization part of manuscript and Abdel-Monien wrote the activity part. Ibrahim and Assirey contributed the manuscript editting and revision and figures drawing. All authors revised the mamnuscript.

Competing interests

The authors declare no competing interests.

Additional information

Supplementary information is available for this paper at https://doi.org/10.1038/s41598-019-55912-2.

Correspondence and requests for materials should be addressed to M.E.M.A. or E.A.A.

Reprints and permissions information is available at www.nature.com/reprints.

Publisher's note Springer Nature remains neutral with regard to jurisdictional claims in published maps and institutional affiliations.